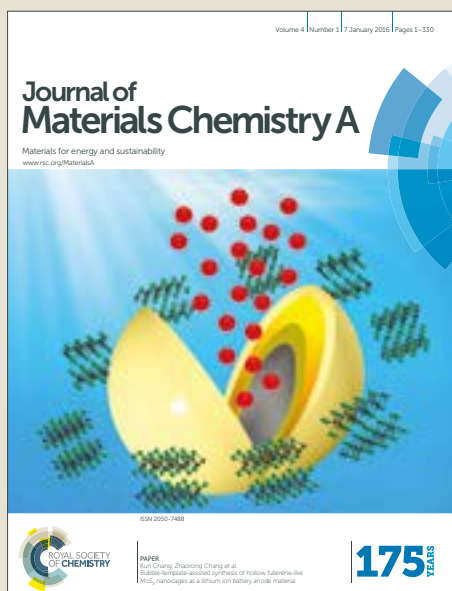


Journal of Materials Chemistry A

Accepted Manuscript



This article can be cited before page numbers have been issued, to do this please use: Y. Chen, B. Shan, C. Yang, J. Yang, J. Li and B. Mu, *J. Mater. Chem. A*, 2018, DOI: 10.1039/C8TA02845A.



This is an Accepted Manuscript, which has been through the Royal Society of Chemistry peer review process and has been accepted for publication.

Accepted Manuscripts are published online shortly after acceptance, before technical editing, formatting and proof reading. Using this free service, authors can make their results available to the community, in citable form, before we publish the edited article. We will replace this Accepted Manuscript with the edited and formatted Advance Article as soon as it is available.

You can find more information about Accepted Manuscripts in the [author guidelines](#).

Please note that technical editing may introduce minor changes to the text and/or graphics, which may alter content. The journal's standard [Terms & Conditions](#) and the ethical guidelines, outlined in our [author and reviewer resource centre](#), still apply. In no event shall the Royal Society of Chemistry be held responsible for any errors or omissions in this Accepted Manuscript or any consequences arising from the use of any information it contains.



Journal Name

ARTICLE

Environmentally-Friendly Synthesis of Flexible MOFs $M(\text{NA})_2$ ($M = \text{Zn, Co, Cu, Cd}$) with Large and Regenerable Ammonia Capacity

Yang Chen,^{a,b} Bohan Shan,^b Chengyin Yang,^a Jiangfeng Yang,^a Jinping Li^{*a} and Bin Mu^{*b}

Received 00th January 20xx,
Accepted 00th January 20xx

DOI: 10.1039/x0xx00000x

www.rsc.org/

Two environmentally-friendly and efficient synthesis methods, NH_3 -assisted synthesis and solvent-evaporated conversion, have been developed for the synthesis of a series of $M(\text{NA})_2$ ($M = \text{Zn, Co, Cu, Cd}$; $\text{NA} = \text{nicotinate}$) flexible MOFs. The two-dimensional $M(\text{NA})_2$ ($M = \text{Zn, Co}$) and three-dimensional $M(\text{NA})_2$ ($M = \text{Cu, Cd}$) materials exhibit peculiar structure transformation. These frameworks can be obtained from dehydration of $M(\text{NA})_2(\text{H}_2\text{O})_4$ ($M = \text{Zn, Co, Cu, Cd}$) which are zero-dimensional supramolecular structures. Interestingly, the structural transformation of $M(\text{NA})_2$ ($M = \text{Zn, Co, Cd}$) is reversible after liquid water adsorption. Due to the flexible structure of those MOFs, they exhibit abnormal NH_3 adsorption properties. The two-dimensional $\text{Zn}(\text{NA})_2$ shows a gate-opening behavior for NH_3 adsorption. Its layers opened at the pressure of 0.22 bar in the first cycle, resulting in a two-step NH_3 uptake with a capacity of 10.2 mmol/g at 1 bar. The gate-opening pressure shifted to a lower value with cycles. $\text{Co}(\text{NA})_2$ has a huge NH_3 uptake of 17.5 mmol/g, which is top-ranking among the reported values. For the NH_3 adsorption over $\text{Cu}(\text{NA})_2$ and $\text{Cd}(\text{NA})_2$, the adsorption rates increase and adsorption equilibrium is achieved faster after three cycles. Their maximum capacity at 1 bar is 13.4 and 6 mmol/g, respectively. More importantly, all MOFs can be regenerated under vacuum and heating conditions of 150 °C for 70 min, and they all retained the capacity. The advantages of environmentally-friendly synthesis, large adsorption capacity, and regenerable properties indicate that $M(\text{NA})_2$ ($M = \text{Zn, Co, Cu}$) are promising candidates for NH_3 adsorption.

1. Introduction

The world pays great attention to air pollution, especially in developing countries that are suffering serious $\text{PM}_{2.5}$ (fine particulate matter, with aerodynamic diameters of $<2.5 \mu\text{m}$) and haze.^{1,2} Air purification becomes a long-term challenge with constantly reinforced standards addressing air pollution (greenhouse and toxic gases).³ Ammonia (NH_3) is the most important gaseous alkaline pollutant, which can give severe impact on animal and human health. Furthermore, NH_3 emissions will react with NO_x , SO_2 , etc. to form $\text{PM}_{2.5}$, which seriously endanger public health.⁴⁻⁶ The world releases a large amount of ammonia every year, among which, China contributes the largest 10.2 million tons of emission.⁷ Meanwhile, ammonia is not only an important resource raw material for agriculture and industry, but is also a significant energy storage intermediate and the only carbon-free chemical energy carrier.^{8,9} Therefore, recycling ammonia for utilization has dual significance in environment and energy.

Metal-organic frameworks (MOFs), a new type of porous materials, possess many advantages such as huge specific

surface areas, abundant pore structures, adjustable functional groups and flexible structures.¹⁰⁻¹³ Those features make these materials prime candidates for applications in gas adsorption, gas purification, or heterogeneous catalysis.¹⁴⁻¹⁶ In recent years, MOFs serving as ammonia adsorbent in the field of environment and energy have gradually evolved.¹⁷⁻¹⁹ Yaghi, Long, and Bando groups have investigated many MOFs or COFs (COF-10, BPP-7, Cu-BTC, etc.) possessing good performance in ammonia adsorption.²⁰⁻²² Our team also found some other MOFs ($\text{Cu}(\text{INA})_2$, ZSA-1 and $\text{NH}_2\text{-MIL-53}$) used in ammonia adsorption reflecting some specific properties.²³⁻²⁵ However, some defects like high synthetic cost, low adsorption capacity, irreversible adsorption process, difficult regeneration, and structural collapse factors limit their actual applications. Therefore, it has been a significant challenge to efficiently synthesize MOFs with low cost, high uptake and recyclable performance for ammonia adsorption.

A series of $M(\text{NA})_2$ ($M = \text{Zn, Co, Cu, Cd}$) MOFs are two- or three-dimensional MOFs ($\text{Zn}(\text{NA})_2$ and $\text{Co}(\text{NA})_2$ are 2D; $\text{Cu}(\text{NA})_2$ and $\text{Cd}(\text{NA})_2$ are 3D) which are assembled by metal and nicotinate (Fig. 1). Their synthesis methods and structural properties had been investigated by Lin and Xu.²⁶⁻²⁹ Their flexible properties are found by us that they can be obtained by the dehydration of $M(\text{NA})_2(\text{H}_2\text{O})_4$ ($M = \text{Zn, Co, Cu, Cd}$)³⁰⁻³³ which are zero-dimensional (0D) supramolecular analogue. $M(\text{NA})_2(\text{H}_2\text{O})_4$ ($M = \text{Zn, Co, Cu, Cd}$) can transform to 2D $\text{Zn}(\text{NA})_2$, $\text{Co}(\text{NA})_2$ frameworks and 3D $\text{Cu}(\text{NA})_2$, $\text{Cd}(\text{NA})_2$ frameworks, and the structural transformation are reversible

^a Shanxi Key Laboratory of Gas Energy Efficient and Clean Utilization, Research Institute of Special Chemicals, Taiyuan University of Technology, Taiyuan 030024, Shanxi, China. Email: jpli211@hotmail.com

^b School for Engineering of Matter, Transport, and Energy, Arizona State University, Tempe, AZ 85287, United States. Email: bmu@asu.edu
Electronic Supplementary Information (ESI) available: [PXRD, SEM, IR, EDS and comparison of NH_3 uptake]. See DOI: 10.1039/x0xx00000x

for $M(\text{NA})_2$ ($M = \text{Zn, Co, Cd}$) after water adsorption. Due to the flexible and multi-dimensional structural transforming properties of these MOFs,

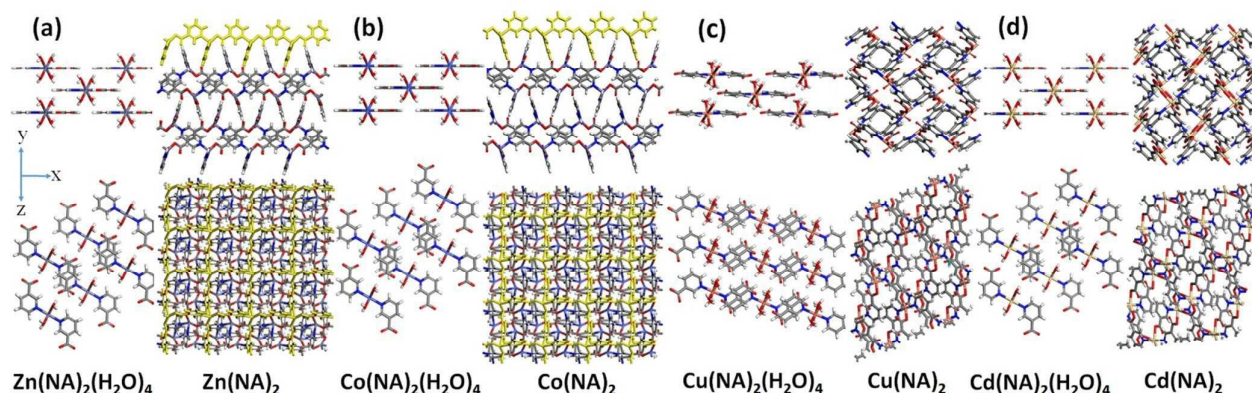


Fig. 1 The structures of $M(\text{NA})_2(\text{H}_2\text{O})_4$ ($M = \text{Zn, Co, Cu, Cd}$) and $M(\text{NA})_2$ ($M = \text{Zn, Co, Cu, Cd}$). The element: grey, C; white, H; red, O; blue, N; navy blue, Zn; royal blue, Co; pink, Cu; khaki, Cd. The yellow is one-layer structure in $\text{Zn}(\text{NA})_2$ and $\text{Co}(\text{NA})_2$.

they exhibit special advantages in the application of ammonia adsorption. Currently, the conventional synthetic methods of $M(\text{NA})_2(\text{H}_2\text{O})_4$ and $M(\text{NA})_2$ ($M = \text{Zn, Co, Cu, Cd}$) require high synthesis temperature, long reaction time and volatile organic solvents. Therefore, it is necessary to push these materials towards practical applications by more green, economic and efficient synthesis methods.

In this work, we report a NH_3 -assisted synthesis method to obtain $M(\text{NA})_2(\text{H}_2\text{O})_4$ ($M = \text{Zn, Co, Cu, Cd}$), which can further transform to $M(\text{NA})_2$ ($M = \text{Zn, Co, Cu, Cd}$) after dehydration. Meanwhile, $M(\text{NA})_2$ can be synthesized by solvent-evaporated conversion (SEC) method as well and both synthetic methods are environmentally-friendly and efficient. The synthesis procedures, structural, flexibility and NH_3 adsorption capabilities of these MOFs are investigated by XRD, TGA, SEM, EDS, IR and $\text{H}_2\text{O}/\text{NH}_3$ adsorption studies. Combining the merits of the improved synthesis methods, high NH_3 uptake, and reversible adsorption process, these materials are promising candidates for NH_3 adsorption.

2. Experimental



Fig. 2 Schematic diagrams of NH_3 -assisted synthesis for $M(\text{NA})_2(\text{H}_2\text{O})_4$ ($M = \text{Zn, Co, Cu, Cd}$) and solvent-evaporated conversion (SEC) syntheses for $M(\text{NA})_2$ ($M = \text{Zn, Co, Cu, Cd}$).

Materials

All reagents were used without further purification. Zinc nitrate hexahydrate ($\text{Zn}(\text{NO}_3)_2 \cdot 6\text{H}_2\text{O}$, 99%) and cadmium nitrate tetrahydrate ($\text{Cd}(\text{NO}_3)_2 \cdot 4\text{H}_2\text{O}$, 99%) were purchased from Aladdin Reagent Co. Ltd.; Cobalt nitrate hexahydrate ($\text{Co}(\text{NO}_3)_2 \cdot 6\text{H}_2\text{O}$, 98%) was obtained from Alfa Aesar; Copper nitrate trihydrate ($\text{Cu}(\text{NO}_3)_2 \cdot 3\text{H}_2\text{O}$, 98 %) was obtained from Sigma-Aldrich; Nicotinic acid (HNA, AR) was purchased from Tianjin Guangfu Fine Chemical Research Institute; Activated carbon (HA-40/50) was purchased from Ningxia Huahui Activated Carbon Co. Ltd.; N,N-dimethylformamide (DMF, 99.7 %), ammonia solution ($\text{NH}_3 \cdot \text{H}_2\text{O}$, 25%) and zeolite Na-4A were obtained from Sinopharm Group Chemical Reagent Co., Ltd. Distilled water (H_2O) was prepared in our laboratory.

NH_3 -assisted synthesis of $M(\text{NA})_2(\text{H}_2\text{O})_4$ ($M = \text{Zn, Co, Cu, Cd}$)

0.615 g HNA (5 mmol) and 12 mL distilled water were mixed in a 20 mL sealed vial. Then 0.27 mL of $\text{NH}_3 \cdot \text{H}_2\text{O}$ (25%) was slowly added into each vial dropwise until HNA completely dissolved. $\text{Zn}(\text{NO}_3)_2 \cdot 6\text{H}_2\text{O}$ (0.743 g, 2.5 mmol), $\text{Co}(\text{NO}_3)_2 \cdot 6\text{H}_2\text{O}$ (0.728 g, 2.5 mmol), $\text{Cu}(\text{NO}_3)_2 \cdot 3\text{H}_2\text{O}$ (0.603 g, 2.5 mmol), or $\text{Cd}(\text{NO}_3)_2 \cdot 4\text{H}_2\text{O}$ (0.77 g, 2.5 mmol) was added into the corresponding vial. The vials were sealed and shocked quickly. The $M(\text{NA})_2(\text{H}_2\text{O})_4$ ($M = \text{Zn, Co, Cd}$) crystals formed immediately, but the large crystals of $\text{Cu}(\text{NA})_2(\text{H}_2\text{O})_4$ formed after 36 hours. The samples were washed with distilled water and dried in air. Yield: $\text{Zn}(\text{NA})_2(\text{H}_2\text{O})_4$, 88.6%; $\text{Co}(\text{NA})_2(\text{H}_2\text{O})_4$, 88.1%; $\text{Cu}(\text{NA})_2(\text{H}_2\text{O})_4$, 90.4%; $\text{Cd}(\text{NA})_2(\text{H}_2\text{O})_4$, 85.7%.

Solvent-evaporated conversion (SEC) of $M(\text{NA})_2$ ($M = \text{Zn, Co, Cu, Cd}$)

Preparation of $M(\text{NA})_2$ ($M = \text{Zn, Cu, Cd}$): $\text{Zn}(\text{NO}_3)_2 \cdot 6\text{H}_2\text{O}$ (0.074 g, 0.25 mmol), $\text{Cu}(\text{NO}_3)_2 \cdot 3\text{H}_2\text{O}$ (0.06 g, 0.25 mmol), or

$\text{Cd}(\text{NO}_3)_2 \cdot 4\text{H}_2\text{O}$ (0.077 g, 0.25 mmol) was evenly mixed with HNA (0.062 g, 0.5 mmol). The mixed powder was placed in a small beaker containing 2 mL of DMF. Each beaker was supported by 20 g of dehydrated activated carbon in 100 mL Teflon-lined autoclave. Crystallization was carried out at 180 °C for 4 hours. Then the autoclaves are cooled to room temperature. The crystals were washed with DMF and dried in air. Preparation of $\text{Co}(\text{NA})_2$: An evenly mixed powder of $\text{Co}(\text{NO}_3)_2 \cdot 6\text{H}_2\text{O}$ (0.073 g, 0.25 mmol) and HNA (0.062 g, 0.5 mmol) was placed in a small beaker, containing 2 mL of distilled water and $\text{NH}_3 \cdot \text{H}_2\text{O}$ (25%) (50 μL). The beaker was supported by 40 g of dehydrated zeolite Na-4A in 100 mL Teflon-lined autoclave. The autoclave was maintained at 80 °C for 4 hours and then heated at 180 °C for 1 hour. The crystals were obtained after cooling. Yield: $\text{Zn}(\text{NA})_2$, 91.7%; $\text{Co}(\text{NA})_2$, 92.4%; $\text{Cu}(\text{NA})_2$, 89.5%; $\text{Cd}(\text{NA})_2$, 90.9%.

Characterization of the samples

The crystallinity and phase purity of the materials were measured by powder X-ray diffraction (PXRD) on a Rigaku Mini Flex II X-ray diffractometer with $\text{Cu-K}\alpha$ radiation operated at 30 kV and 15 mA. Scanning was performed over the 2θ range of 5–40° at 4°/min. Scanning electron microscopy (SEM) images and EDS spectra were obtained using a Hitachi SEM (SU8010, Hitachi, Japan) equipped with a Horiba X-Max 50 EDX system. The TGA of the samples was collected on a thermal analyzer (NETZSCH, STA 449 F5) at a heating rate of 10 °C/min under an air atmosphere. CO_2 adsorption/desorption isotherms were obtained using an ASAP 2460 Surface Area and Porosity Analyzer at 0 °C. The infrared (IR) spectra were recorded on an FT-IR8400S spectrometer. Water vapor adsorption on the samples was determined by vapor sorption measurements on an Autosorb-iQ Quantachrome (volumetric technique) with a vapor generator at 25 °C.

NH_3 adsorption and desorption measurements

In the NH_3 adsorption measurements, the purity of NH_3 was 99.999%. The samples were activated at 150 °C for $\text{M}(\text{NA})_2(\text{H}_2\text{O})_4$ (M=Zn, Cu, Cd) and 200 °C for $\text{Co}(\text{NA})_2(\text{H}_2\text{O})_4$ overnight under vacuum or until no further weight loss was observed. The adsorption isotherms for NH_3 were collected on an Intelligent Gravimetric Analyzer (IGA 001, Hiden, UK). Adsorption equilibrium data was collected once a stable pressure (more than 8 adsorption points were recorded from 0 to 1 bar) and weight was maintained for 30 min to reach an adsorption equilibrium at each point along the isotherm. All the NH_3 adsorption isotherms were collected at 25 °C, and samples were activated under vacuum and 150 °C for 70 min in each cycle.

3. Results and discussion

In reported literatures,^{30–33} high reaction temperature (at least 150 °C) or long reaction time (more than 3 days) are usually necessary in the synthetic process of $\text{M}(\text{NA})_2(\text{H}_2\text{O})_4$ (M=Zn, Co, Cu, Cd). However, through the method of NH_3 -assisted

synthesis, we can bring this requirement down to room temperature. The reaction time for synthesizing $\text{M}(\text{NA})_2(\text{H}_2\text{O})_4$ (M=Zn, Co, Cd) is reduced to less than 5 min and for $\text{Cu}(\text{NA})_2(\text{H}_2\text{O})_4$, this number is brought down to 36 h, while having the yields over 85%. As shown in Fig. 3, the PXRD patterns of synthesized $\text{M}(\text{NA})_2(\text{H}_2\text{O})_4$ (M=Zn, Co, Cu, Cd) are matched well with their simulated patterns, indicating the

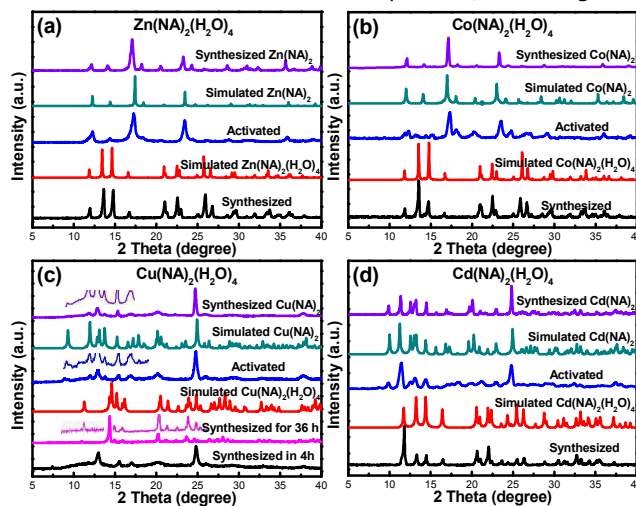


Fig. 3 The synthesized and activated PXRD patterns of $\text{M}(\text{NA})_2(\text{H}_2\text{O})_4$ (M = Zn, Co, Cu, Cd) and compared with $\text{M}(\text{NA})_2$ (M = Zn, Co, Cu, Cd). PXRD patterns of $\text{Cu}(\text{NA})_2$ insert partial enlargement.

successful syntheses. Amine regulators^{34–36} (ammonia, dimethylamine, trimethylamine, etc.) are usually used in the synthesis of MOFs to adjust the pH of solution, dissolution of ligands, coordination environment, reaction speed or crystal size. In our synthesis system, due to the addition of $\text{NH}_3 \cdot \text{H}_2\text{O}$ which can induce rapid crystallization of the precursors³⁷, HNA can be completely dissolved in water resulting in a large number existence of NA^- in alkaline environment. When the metal salts were added into the solution, dissolved metal ions coordinated with the NA^- and H_2O rapidly in ammonia collaborative coordination environment and formed $\text{M}(\text{NA})_2(\text{H}_2\text{O})_4$ (M=Zn, Co, Cu, Cd) at last. As shown in Fig. 3c and Fig. S1, a different phenomenon was observed in the synthesis of $\text{Cu}(\text{NA})_2(\text{H}_2\text{O})_4$. Precursor was formed in the first 4 h of crystallization process. Then the precursor gradually transformed to dark blue crystals of $\text{Cu}(\text{NA})_2(\text{H}_2\text{O})_4$ in the next 32 h of reaction. $\text{M}(\text{NA})_2(\text{H}_2\text{O})_4$ (M=Zn, Co, Cu, Cd) has a 0D supramolecular analogue structure which can coordinate with four H_2O molecules. After activation, these materials transformed to $\text{M}(\text{NA})_2$ (M=Zn, Co, Cu, Cd) with a huge structural change. As a result, 0D $\text{M}(\text{NA})_2(\text{H}_2\text{O})_4$ (M=Zn, Co, Cu, Cd) were changed to $\text{M}(\text{NA})_2$ (M=Zn, Co) with 2D layer structures and $\text{M}(\text{NA})_2$ (M= Cu, Cd) with 3D frameworks. The transformation from $\text{M}(\text{NA})_2(\text{H}_2\text{O})_4$ to $\text{M}(\text{NA})_2$ is confirmed by the PXRD patterns in Fig. 3. In addition, $\text{M}(\text{NA})_2$ (M=Zn, Co, Cu, Cd) can be directly synthesized by another environmentally-friendly synthesis method (SEC)³⁸ in 4 h. In the SEC method, activated carbon or zeolite served as a medium to load evaporated solvent, which can increase the concentration of

reactants resulting in fast reaction rates. In the meantime, the volatile organic solvents could be adsorbed in activated carbon for reuse and avoiding pollution.³⁹ The synthesis results are shown in Fig. 3 that $M(\text{NA})_2$ ($M=\text{Zn}, \text{Co}, \text{Cu}, \text{Cd}$) were synthesized successfully. In order to research the flexible transformation properties of this materials in the following, we mainly used the $M(\text{NA})_2$ ($M=\text{Zn}, \text{Co}, \text{Cu}, \text{Cd}$) samples obtained from dehydrated $M(\text{NA})_2(\text{H}_2\text{O})_4$ ($M=\text{Zn}, \text{Co}, \text{Cu}, \text{Cd}$).

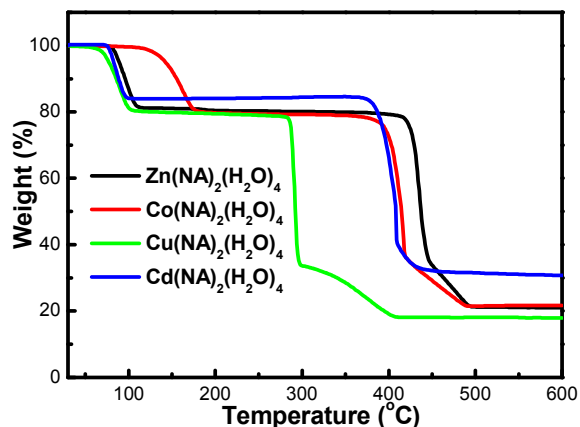


Fig. 4 TGA data for $M(\text{NA})_2(\text{H}_2\text{O})_4$ ($M = \text{Zn}, \text{Co}, \text{Cu}, \text{Cd}$).

TGA data of $M(\text{NA})_2(\text{H}_2\text{O})_4$ ($M=\text{Zn}, \text{Co}, \text{Cu}, \text{Cd}$) were recorded to investigate their thermal stability and activation temperature of flexible transformation. As seen in Fig. 4, the four materials all exhibited two weight loss stages. The first weight loss of $M(\text{NA})_2(\text{H}_2\text{O})_4$ ($M=\text{Zn}, \text{Cu}, \text{Cd}$) occurred at temperature about 80–120 °C. The one of $\text{Co}(\text{NA})_2(\text{H}_2\text{O})_4$ happened at 120–180 °C. In the first stage, the weight loss of $\text{Cd}(\text{NA})_2(\text{H}_2\text{O})_4$ is 18% and all the others have about 20%. This can be attributed to the higher mass fraction of Cd. The amounts of the first weight loss are consistent with their coordinated H_2O contents. Therefore, this stage is the dehydration process of $M(\text{NA})_2(\text{H}_2\text{O})_4$ ($M=\text{Zn}, \text{Co}, \text{Cu}, \text{Cd}$), indicating $M(\text{NA})_2$ ($M=\text{Zn}, \text{Co}, \text{Cu}, \text{Cd}$) can be obtained from $M(\text{NA})_2(\text{H}_2\text{O})_4$ ($M=\text{Zn}, \text{Co}, \text{Cu}, \text{Cd}$) being activated at 150 °C and $\text{Co}(\text{NA})_2(\text{H}_2\text{O})_4$ being activated at 200 °C. After a long plateau, $M(\text{NA})_2(\text{H}_2\text{O})_4$ ($M=\text{Zn}, \text{Co}, \text{Cd}$) and $\text{Cu}(\text{NA})_2(\text{H}_2\text{O})_4$ have the second weight loss at temperatures of 400–500 °C and 300–400 °C, respectively, which are attributed to the framework collapse. Thus, $M(\text{NA})_2$ have great thermal stability that can retain their structural integrity till at least 300 °C, and $M(\text{NA})_2$ ($M=\text{Zn}, \text{Co}, \text{Cd}$) can even withstand up to 400 °C.

Because $M(\text{NA})_2(\text{H}_2\text{O})_4$ ($M=\text{Zn}, \text{Co}, \text{Cu}, \text{Cd}$) can transform to $M(\text{NA})_2$ ($M=\text{Zn}, \text{Co}, \text{Cu}, \text{Cd}$), their water adsorption isotherms were collected to study the reversible transform process. Water vapor adsorption isotherms of these four MOFs are shown in Fig. 5. The isotherms of $\text{Zn}(\text{NA})_2$ is almost flat, which indicates $\text{Zn}(\text{NA})_2$ almost does not adsorb H_2O . $\text{Cu}(\text{NA})_2$ and $\text{Cd}(\text{NA})_2$ have small H_2O adsorption capacity at low relative pressure, and these values slightly increase to 35 and 56 cc/g, respectively. $\text{Co}(\text{NA})_2$ also has small H_2O adsorption amount under the relative pressure of 0.8. When the relative pressure

increases to 0.9, the adsorption amount has a huge increase to 237 cc/g. As can be seen from the desorption isotherms, the adsorbed H_2O in $M(\text{NA})_2$ ($M=\text{Zn}, \text{Cu}, \text{Cd}$) can be desorbed with the pressure drop. However, the desorption branch of H_2O on $\text{Co}(\text{NA})_2$ is almost unchanged indicating that H_2O is strongly bound to $\text{Co}(\text{NA})_2$. The PXRD patterns in Fig. S2 also demonstrated the strong effects of H_2O on the crystal structural of $\text{Co}(\text{NA})_2$. After water vapor adsorption, the PXRD patterns of $M(\text{NA})_2$ ($M=\text{Zn}, \text{Cu}, \text{Cd}$) show no change, but that of $\text{Co}(\text{NA})_2$ has a new pattern, which is consistent with the PXRD

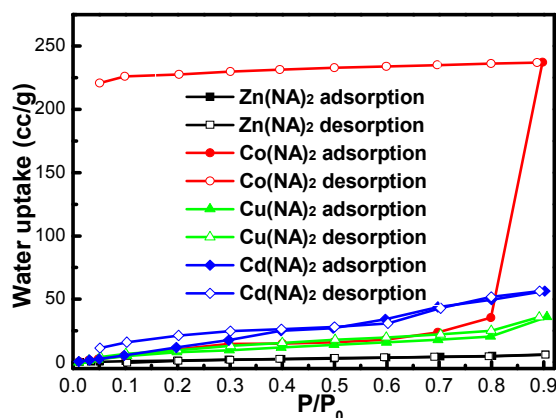


Fig. 5 Water vapor adsorption-desorption of $M(\text{NA})_2$ ($M = \text{Zn}, \text{Co}, \text{Cu}, \text{Cd}$) at 25 °C. Solid points represent adsorption data; hollow points represent desorption data.

$\text{Co}(\text{NA})_2(\text{H}_2\text{O})_4$. Therefore, in the water vapor adsorption, $M(\text{NA})_2$ ($M=\text{Zn}, \text{Cu}, \text{Cd}$) were physical adsorption in pores, but $\text{Co}(\text{NA})_2$ transformed to $\text{Co}(\text{NA})_2(\text{H}_2\text{O})_4$ through chemical adsorption of H_2O . Furthermore, Fig. S2 also reflects their transform properties in liquid water, $M(\text{NA})_2$ ($M=\text{Zn}, \text{Co}, \text{Cd}$) all can transform to $M(\text{NA})_2(\text{H}_2\text{O})_4$ ($M=\text{Zn}, \text{Co}, \text{Cd}$), but the PXRD pattern of $\text{Cu}(\text{NA})_2$ still has no change. Since this series of MOF materials has the same ligand and similar topology, the different macroscopic properties are due to the different microstructures. We can see from Fig. S3 that $\text{Cu}(\text{NA})_2$ has shortest M–O and M–N bonds. So, it's hard for H_2O to attack Cu sites. In contrast, $\text{Co}(\text{NA})_2$ have relatively long bonds, so its structure is easy influenced by both gaseous or liquid water. In brief, $M(\text{NA})_2$ ($M=\text{Zn}, \text{Cd}$) can transform to $M(\text{NA})_2(\text{H}_2\text{O})_4$ ($M=\text{Zn}, \text{Cd}$) in liquid water, $\text{Co}(\text{NA})_2$ can transform to $\text{Co}(\text{NA})_2(\text{H}_2\text{O})_4$ both in liquid water and water vapor, $\text{Cu}(\text{NA})_2$ has a very stable structure and is not influenced by water.

In order to investigate the specific surface area and pore-size distribution of $M(\text{NA})_2$ ($M = \text{Zn}, \text{Co}, \text{Cu}, \text{Cd}$), their CO_2 adsorption were conducted at 0 °C. As shown in Fig. 6, $\text{Zn}(\text{NA})_2$ has the largest CO_2 adsorption capacity of 13.4 cm^3/g at 1 bar; $\text{Cu}(\text{NA})_2$ has the capacity of 6.9 cm^3/g ; $\text{Co}(\text{NA})_2$ and $\text{Cd}(\text{NA})_2$

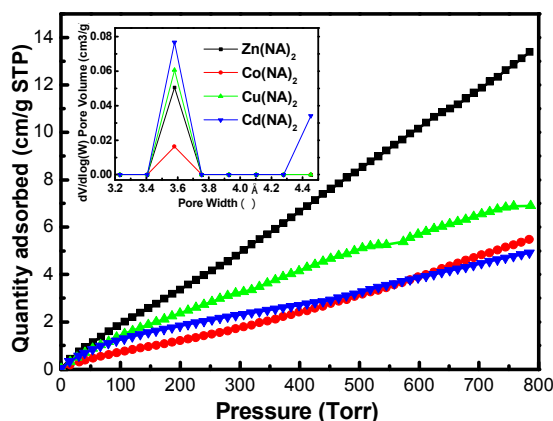


Fig. 6 CO₂ adsorption at 0 °C and pore-size distribution of M(NA)₂ (M = Zn, Co, Cu, Cd). Black, Zn(NA)₂; red, Co(NA)₂; green, Cu(NA)₂; blue, Cd(NA)₂.

lower capacity of about 5 cm³/g. The CO₂ adsorption amounts correspond to the BET surface area of M(NA)₂ (M = Zn, Co, Cu, Cd), which are 104, 55, 74 and 41 m²/g, respectively. Pore-size distributions of M(NA)₂ (M = Zn, Co, Cu, Cd) are shown in the inset-graph of Fig. 6. The four MOFs all have small pore size around 3.8 Å, and Cd(NA)₂ also has pores around 4.4 Å. Due to the small BET surface area and pore size of M(NA)₂ (M = Zn, Co, Cu, Cd), these MOFs show a limited potential for adsorption of larger molecules. However, NH₃ is a strong polar gas with a small kinetic diameter (2.9 Å).⁴⁰ Special adsorption configurations and adsorption sites are usually more important than big surface area and pore factors in NH₃ adsorption.^{41,42} Thus, flexible structure, small pore and adsorption sites are the major factors to consider in NH₃ adsorption on M(NA)₂ (M = Zn, Co, Cu, Cd).

The SEM images of as-synthesized, activated, and NH₃ adsorbed samples are shown in Fig. S4. The as-synthesized M(NA)₂(H₂O)₄ (M = Zn, Co, Cu, Cd) are crystals with smooth surface. Zn(NA)₂ is a rod-shaped structure with a length about 15 μm. Co(NA)₂ is an irregular rod-like structure with about 10 μm length. Cu(NA)₂ has a big monoclinic structure with length × width about 150 × 200 μm. The shape of Cd(NA)₂ is a layered structure with ~1 μm thickness. After the dehydration process of M(NA)₂(H₂O)₄ transforming to M(NA)₂, their internal structures have a regular rearrangement. These MOFs maintained their original shapes, and the only variation is their surfaces become rough due to H₂O removing from their structures. However, their surfaces have significant changes after NH₃ adsorption, Zn(NA)₂ becomes rougher, Co(NA)₂ crystals become rounded and coalesce together. The surfaces of Cu(NA)₂ and Cd(NA)₂ are cracked. In order to get more information about these changes, EDS and IR spectra analyses were conducted and results are shown in Fig. 7, Fig. S5 and Fig. S6. The EDS spectrums show the changes of nitrogen element ratio (N/O) in their structural transformation. In the process of M(NA)₂(H₂O)₄ transforming to M(NA)₂, nitrogen element has a slight increase due to the decrease of water ratio in structures.

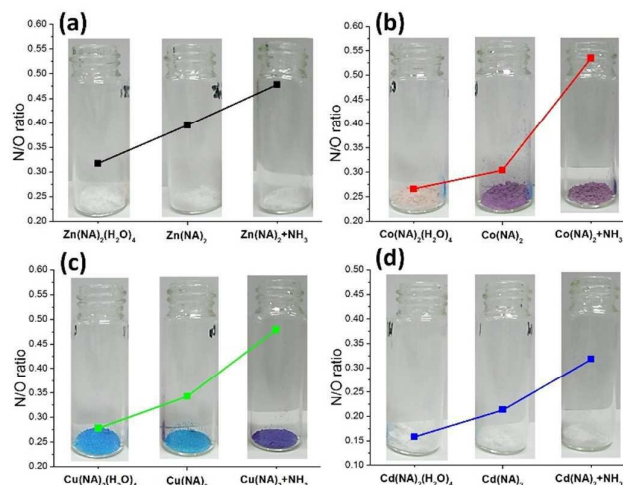


Fig. 7 Evolution of the macroscopic color and N/O ratio of M(NA)₂(H₂O)₄ (M = Zn, Co, Cu, Cd) that as-synthesized, activated and adsorbed NH₃.

After NH₃ adsorption, the ratio of nitrogen element in Zn(NA)₂ and Cd(NA)₂ also have slightly increased, but that of Co(NA)₂ and Cu(NA)₂ have increased the most indicating that they have a large NH₃ adsorption capacity. In the transform process, the colour of Zn(NA)₂ and Cd(NA)₂ gradually grayed out. Co(NA)₂ changed from pink to purple, and Cu(NA)₂ became dark blue eventually (Fig. 7). These MOFs share the same functional group so that the different properties are owing to metal nodes and microstructures. In the IR spectra of these MOFs (Fig. S6), the peaks appeared between 500 and 2000 cm⁻¹ are due to the nicotinate ligands and remained the same, but the changed peaks between 3000 and 3800 cm⁻¹ can reflect the removal of H₂O and NH₃ adsorption process. M(NA)₂(H₂O)₄ (M = Zn, Co, Cu, Cd) showed a wide IR peak for H₂O adsorption at 3200–3600 cm⁻¹, but this peak disappeared after H₂O molecules were removed. Moreover, M(NA)₂ (M = Zn, Co, Cu, Cd) have shown many strong vibration peaks of coordinated NH₃ molecules at ~3300 cm⁻¹ after the adsorption of NH₃,⁴³ which indicates those MOFs can indeed uptake a lot of NH₃ molecules.

In order to investigate the NH₃ reversible uptake over M(NA)₂ (M = Zn, Co, Cu, Cd), three cycles of NH₃ adsorption-desorption tests were conducted and the results are shown in Fig. 8. The adsorption-desorption isotherm of Zn(NA)₂ (Fig. 8a) shows that, when below 0.22 bar, the NH₃ adsorption capacity in the first cycle only has slight increase with increasing pressure. However, when the pressure increases to 0.4 bar, the adsorption amount has a huge jump to 10.2 mmol/g. This type of adsorption isotherm represents a typical gate-opening behavior, which can be explained by its particular layer structures.^{44,45} Zn(NA)₂ has a 2D layered structure with small pores and interplanar spacing. When the pressure was below 0.22 bar, it had little space to adsorb NH₃, resulting in a small adsorption amount (< 1 mmol/g). When the pressure is further increased, its layers were opened and filled with a large amount of NH₃. As a result, the isotherm reached to

adsorption equilibrium (10.2 mmol/g) quickly. After NH_3 adsorption, the PXRD pattern (Fig. S7a) of $\text{Zn}(\text{NA})_2$ showed

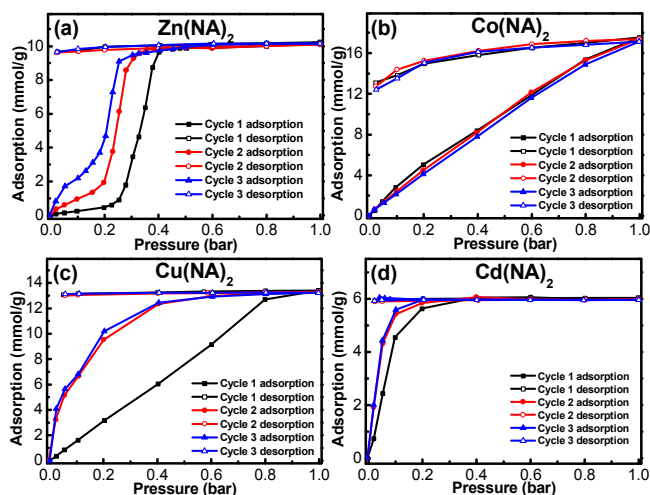


Fig. 8 Three cycle curves for NH_3 adsorption onto $\text{M}(\text{NA})_2$ ($\text{M} = \text{Zn}, \text{Co}, \text{Cu}, \text{Cd}$) at 25°C . Materials were regenerated at 150°C and vacuum for 70 min in each cycle. The solid point is the adsorption point, the hollow point is the desorption point.

that some main peaks were changed or shifted, and some extra speaks appeared at low 2θ , which indicate the layer space had opened and pores were enlarged, resulting in a large NH_3 uptake. As can be found in the second and third adsorption isotherms of $\text{Zn}(\text{NA})_2$, the open pressure shifted to lower values, indicating that the MOF layers can be more easily expanded than the original one. After three cycles, the structures became more flexible and could reach adsorption equilibrium more quickly, while the maximum adsorption amount has not changed. The three adsorption cycles of $\text{Co}(\text{NA})_2$ are shown in Fig. 8b, the adsorption amount increases with the increasing pressure, and the maximum uptake is up to 17.5 mmol/g, which is among the highest reported values. As can be seen from PXRD pattern in Fig. S7b, $\text{Co}(\text{NA})_2$ shows no peaks after NH_3 adsorption, indicating that NH_3 has a strong impact on the long-range order of $\text{Co}(\text{NA})_2$ crystal. Its structure experienced an order-disorder transition from crystalline to amorphous, which is similar to the transformation of crystalline structures to amorphous MOF.^{46,47} In the water vapor adsorption of $\text{Co}(\text{NA})_2$, its structure is sensitive to H_2O , and its structure has long M-O and M-N bonds (Fig. S3), so the structure of $\text{Co}(\text{NA})_2$ can be easy transformed, which implies NH_3 as another strong polar molecular can easily enter and influence its structure as well. Just like $\text{Co}(\text{NA})_2$, amorphous transition also occurs in the ammonia adsorption of other MOFs ($\text{Co}_2\text{Cl}_2\text{BBTA}$). Though ammonia cause its structure collapses, it does not predict a decline in the ammonia uptake; rather, the interaction strength between bonding sites and ammonia is a more important predictor of ammonia uptake.⁴² In ammonia adsorption of $\text{Co}(\text{NA})_2$, its changed layers became amorphous cobalt and nicotinate fragments which exposes many open sites of metal.²³ As a result, it reflected a large and equivalent adsorption capacity in three cycles. In the NH_3 adsorption of $\text{Cu}(\text{NA})_2$ and $\text{Cd}(\text{NA})_2$ (Fig. 8c and Fig. 8d), the first isotherms are lower than that of the second and third

mainly due to their small surface area and pore size. After regeneration, the adsorbed NH_3 are removed from pores. The first adsorption-desorption cycle leads to smooth channels and memory effect.^{23,48} Therefore, the adsorption rates increase, and adsorption equilibrium is achieved faster in the second and third cycles. From their PXRD patterns after NH_3 adsorption (Fig. S7), same changes of peaks also occurred, which is a common phenomenon in NH_3 adsorption for many MOFs.⁴⁹ Among them, $\text{Cu}(\text{NA})_2$ shows slight change of peaks indicating its stable structure. However, $\text{Cd}(\text{NA})_2$ has changeable structure with long M-O and M-N bonds, its PXRD peaks have large offset after NH_3 adsorption. The structure of $\text{Cd}(\text{NA})_2$ may undergo some degree of structural distortion and transformation.⁵⁰ The final adsorption amount of $\text{Cu}(\text{NA})_2$ and $\text{Cd}(\text{NA})_2$ are about 13.4 mmol/g and 6 mmol/g, respectively. The adsorption capacities of this materials did not decrease after three cycles.

The regeneration properties of porous materials are significant for the adsorption application. As shown in the plot of the adsorption-desorption isotherms, most adsorbed NH_3 did not desorb with the pressure decrease except in the case of $\text{Co}(\text{NA})_2$, indicating most NH_3 molecules are chemisorbed to the frameworks. Therefore, high temperature regeneration

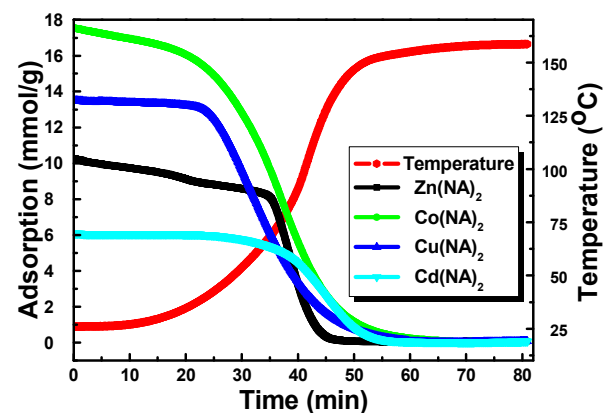


Fig. 9 NH_3 removal curves of $\text{M}(\text{NA})_2$ ($\text{M} = \text{Zn}, \text{Co}, \text{Cu}, \text{Cd}$) against time and temperature.

was carried out in each cycle and the NH_3 desorption curves were showed in Fig. 9. As the temperature gradually increases to 150°C under vacuum, NH_3 can be almost completely removed from the examined MOFs. Comparing with the adsorption and desorption amount, NH_3 removal rate of $\text{M}(\text{NA})_2$ ($\text{M} = \text{Zn}, \text{Co}, \text{Cu}, \text{Cd}$) are 98.9%, 99.4%, 98.8%, 98.6%, separately. $\text{Zn}(\text{NA})_2$ and $\text{Co}(\text{NA})_2$ started NH_3 desorption after 20 min at 30°C . The NH_3 removal speed of $\text{Co}(\text{NA})_2$ and $\text{Cu}(\text{NA})_2$ are increased after 50°C . $\text{Zn}(\text{NA})_2$ and $\text{Cd}(\text{NA})_2$ exhibit a considerable extent of NH_3 removal above 80°C , and the adsorbed NH_3 are completely removed after 70 min at about 150°C . Thus, efficient regeneration of the four MOFs can be achieved by heating to 150°C in vacuum for at least 70 min. A summary and comparison of NH_3 uptake at different conditions, regeneration and adsorption loss of reported

porous materials are listed in Table S1. It can be seen from the comparison that Zn(NA)₂, Co(NA)₂ and Cu(NA)₂ have large NH₃ uptake of more than 10 mmol/g (1 bar, 25 °C), especially the adsorption capacity of Co(NA)₂ is top-ranking at the similar pressure and temperature conditions, though many reported materials were tested at 20 °C. More importantly, the four MOFs have reusable advantages over many other non-regenerable MOFs (Cu-BTC, MOF-5, MOF-177 etc.).^{51,52}

4. Conclusions

With the continuous concerns of ammonia treatment from the air pollution and clean energy perspectives, the employment of porous materials in ammonia adsorption is of great significance. We have used NH₃-assisted synthesis and solvent-evaporated conversion to synthesize a series of MOFs, M(NA)₂ (M = Zn, Co, Cu, Cd), they exhibit the structural flexibility, allowing the interconversion to M(NA)₂(H₂O)₄ (M = Zn, Co, Cu, Cd). These flexible MOFs with similarity in synthetic and structure transformation, however, have demonstrated differences in microstructure and adsorption performance. Zn(NA)₂ and Co(NA)₂ with layered structures have particular NH₃ adsorption performance. Zn(NA)₂ has two-step NH₃ adsorption and Co(NA)₂ has a continually increased and huge NH₃ uptake. The adsorption of Cu(NA)₂ and Cd(NA)₂ become fast and tend to be stable after three cycles. Due to their flexible properties, M(NA)₂ (M = Zn, Co, Cu, Cd) have large NH₃ uptakes of 10.2, 17.5, 13.4 and 6 mmol/g, respectively. More importantly, under the conditions of vacuum and heating at 150 °C for 70 min, these materials could be efficient regenerated without loss of performance. Therefore, due to the advantages of flexible structures, high ammonia uptake and reusable performance, M(NA)₂ (M = Zn, Co, Cu) have potential application in ammonia adsorption.

Acknowledgements

We show great gratitude to the National Natural Science Foundation of China (No. 21676175), the Graduate Education Innovation Project of Shanxi Province (No. 2017BY051), and the State Scholarship Fund from China Scholarship Council (No. 201706930002)..

Notes and references

- Q. Zhang, X. Jiang, D. Tong, S. J. Davis, H. Zhao, G. Geng, T. Feng, B. Zheng, Z. Lu, D. G. Streets, R. Ni, M. Brauer, A. van Donkelaar, R. V. Martin, H. Huo, Z. Liu, D. Pan, H. Kan, Y. Yan, J. Lin, K. He and D. Guan, *Nature*, 2017, **543**, 705-709.
- B. Khalid, X. Bai, H. Wei, Y. Huang, H. Wu and Y. Cui, *Nano Lett.*, 2017, **17**, 1140-1148.
- J. Lelieveld, U. Pöschl, *Nature*, 2017, **551**, 291-293.
- J. Heo, S. T. McCoy and P. J. Adams, *Environ. Sci. Technol.*, 2015, **49**, 5142-5150.
- F. T. U. Kohler, S. Popp, H. Klefer, I. Eckle, C. Schrage, B. Böhringer, D. Roth, M. Haumann and P. Wasserscheid, *Green Chem.*, 2014, **16**, 3560.

- J. Zhang, D. Yue, T. Xia, Y. Cui, Y. Yang and G. Qian, *Microporous Mesoporous Mater.*, 2017, **253**, 146-150.
- F. Paulot, D. J. Jacob, R. Pinder, J. Bash, K. Travis and D. Henze, *J. Geophys. Res.: Atmos.*, 2014, **119**, 4343-4364.
- L. Wang, Y. Yi, Y. Zhao, R. Zhang, J. Zhang and H. Guo, *ACS Catal.*, 2015, **5**, 4167-4174.
- B. Cui, J. Zhang, S. Liu, X. Liu, W. Xiang, L. Liu, H. Xin, M. J. Lefler and S. Licht, *Green Chem.*, 2017, **19**, 298-304.
- M. Eddaoudi, J. Kim, N. Rosi, D. Vodak, J. Wachter, M. O'keeffe and O. M. Yaghi, *Science*, 2002, **295**, 469-472.
- P. G. Yot, Q. Ma, J. Haines, Q. Yang, A. Ghoufi, T. Devic, C. Serre, V. Dmitriev, G. Férey, C. Zhong and G. Maurin, *Chem. Sci.*, 2012, **3**, 1100.
- S. Couck, J. F. Denayer, G. V. Baron, T. Rémy, J. Gascon and F. Kapteijn, *J. Am. Chem. Soc.*, 2009, **131**, 6326-6327.
- B. Ilić and S. G. Wettstein, *Microporous Mesoporous Mater.*, 2017, **239**, 221-234.
- L. A. Darunte, A. D. Oetomo, K. S. Walton, D. S. Sholl and C. W. Jones, *ACS Sustainable Chem. Eng.*, 2016, **4**, 5761-5768.
- H. Huang, W. Zhang, F. Yang, B. Wang, Q. Yang, Y. Xie, C. Zhong and J.-R. Li, *Chem. Eng. J.*, 2016, **289**, 247-253.
- J. Chen, J. Chen and Y. Li, *J. Mater. Chem. A*, 2017, **5**, 24116-24125.
- H. Jasuja, G. W. Peterson, J. B. Decoste, M. A. Browe and K. S. Walton, *Chem. Eng. Sci.*, 2015, **124**, 118-124.
- S. Glomb, D. Woschko, G. Makhlofi and C. Janiak, *ACS Appl. Mater. Interfaces*, 2017, **9**, 37419-37434.
- W. P. Mounfield, M. Taborga Claire, P. K. Agrawal, C. W. Jones and K. S. Walton, *Ind. Eng. Chem. Res.*, 2016, **55**, 6492-6500.
- C. J. Doonan, D. J. Tranchemontagne, T. G. Glover, J. R. Hunt and O. M. Yaghi, *Nat. Chem.*, 2010, **2**, 235-238.
- G. Barin, G. W. Peterson, V. Crocellà, J. Xu, K. A. Colwell, A. Nandy, J. A. Reimer, S. Bordiga and J. R. Long, *Chem. Sci.*, 2017, **8**, 4399-4409.
- C. Petit and T. J. Bandoz, *Adv. Funct. Mater.*, 2010, **20**, 111-118.
- Y. Chen, L. Li, J. Li, K. Ouyang and J. Yang, *J. Hazard. Mater.*, 2016, **306**, 340-347.
- Y. Chen, Y. Wang, C. Yang, S. Wang, J. Yang and J. Li, *ACS Sustainable Chem. Eng.*, 2017, **5**, 5082-5089.
- Y. Chen, F. Zhang, Y. Wang, C. Yang, J. Yang and J. Li, *Microporous Mesoporous Mater.*, 2017, **258**, 170-177.
- W. Lin, O. R. Evans, R.-G. Xiong and Z. Wang, *J. Am. Chem. Soc.*, 1998, **120**, 13272-13273.
- W.-J. Feng, G.-P. Zhou, X.-F. Zheng, Y.-G. Liu and Y. Xu, *Acta Crystallogr.*, 2006, **E62**, m2033-m2035.
- M. E. Chapman, P. Ayyappan, B. M. Foxman, G. T. Yee and W. Lin, *Cryst. Growth Des.*, 2001, **1**, 159-163.
- O. R. Evans and W. Lin, *Chem. Mater.*, 2001, **13**, 3009-3017.
- J. Lu, K. Zhao, Q.-R. Fang, J.-Q. Xu, J.-H. Yu, X. Zhang, H.-Y. Bie and T.-G. Wang, *Cryst. Growth Des.*, 2005, **5**, 1091-1098.
- J.-H. Yu, J. Lu, Y. Xu, X. Zhang and J.-Q. Xu, *Inorg. Chim. Acta*, 2006, **359**, 3205-3211.
- A. Kenar, C. Arici, O. Atakol and D. Ülkü, *Anal. Sci.*, 1999, **15**, 399-400.
- Y. Zhou, W. Bi, X. Li, J. Chen, R. Cao and M. Hong, *Acta Crystallogr.*, 2003, **E59**, m356-m358.
- Y. Chen, C. Yang, X. Wang, J. Yang, K. Ouyang and J. Li, *J. Mater. Chem. A*, 2016, **4**, 10345-10351.
- X. Jia, N. Yuan, L. Wang, J. Yang and J. Li, *Eur. J. Inorg. Chem.*, 2018, **2018**, 1047-1052.
- Z. Wang, S. Hu, J. Yang, A. Liang, Y. Li, Q. Zhuang and J. Gu, *Adv. Funct. Mater.* 2018, 1707356
- K. Shen, L. Zhang, X. Chen, L. Liu, D. Zhang, Y. Han, J. Chen, J. Long, R. Luque, Y. Li and B. Chen, *Science*, 2018, **359**, 206-210.

ARTICLE

Journal Name

- 38 Y. Chen, C. Yang, X. Wang, J. Yang and J. Li, *Chem. Eng. J.*, 2017, **313**, 179-186.
- 39 B. Yuan, M. Shao, S. Lu and B. Wang, *Atmos. Environ.*, 2010, **44**, 1919-1926.
- 40 J. R. Li, R. J. Kuppler and H. C. Zhou, *Chem. Soc. Rev.*, 2009, **38**, 1477-1504.
- 41 K. Vikrant, V. Kumar, K.-H. Kim and D. Kukkar, *J. Mater. Chem. A*, 2017, **5**, 22877-22896.
- 42 A. J. Rieth and M. Dinca, *J. Am. Chem. Soc.*, 2018, **140**, 3461-3466.
- 43 T. Ahnfeldt, D. Gunzelmann, T. Loiseau, D. Hirsemann, J. r. Senker, G. Férey and N. Stock, *Inorg. Chem.*, 2009, **48**, 3057-3064.
- 44 S. Sakaida, K. Otsubo, O. Sakata, C. Song, A. Fujiwara, M. Takata and H. Kitagawa, *Nat. Chem.*, 2016, **8**, 377-383.
- 45 R. Kitaura, K. Seki, G. Akiyama and S. Kitagawa, *Angew. Chem., Int. Ed.*, 2003, **42**, 428-431.
- 46 S. Horike and S. Kitagawa, *Nat. Mater.*, 2017, **16**, 1054-1055.
- 47 R. Gaillac, P. Pullumbi, K. A. Beyer, K. W. Chapman, D. A. Keen, T. D. Bennett and F. X. Coudert, *Nat. Mater.*, 2017, **16**, 1149-1154.
- 48 E. R. Engel, A. Jouaiti, C. X. Bezuidenhout, M. W. Hosseini and L. J. Barbour, *Angew. Chem., Int. Ed.*, 2017, **56**, 8874-8878.
- 49 E. Borfecchia, S. Maurelli, D. Gianolio, E. Groppo, M. Chiesa, F. Bonino and C. Lamberti, *J. Phys. Chem. C*, 2012, **116**, 19839-19850.
- 50 C. Chen, L. X. Cai, B. Tan, Y. J. Zhang, X. D. Yang and J. Zhang, *Chem. Commun.*, 2015, **51**, 8189-8192.
- 51 L. Huang, T. Bandoz, K. L. Joshi, A. C. van Duin and K. E. Gubbins, *J. Chem. Phys.*, 2013, **138**, 034102.
- 52 D. Saha and S. Deng, *J. Colloid Interface Sci.*, 2010, **348**, 615-620.

Graphic Abstract

